electronics

MDPI

Article

Evaluation and Comprehensive Comparison of H-Bridge-Based Bidirectional Rectifier and Unidirectional Rectifiers

Jiaqing Deng, Hong Cheng *, Cong Wang, Shiyan Wu and Mingjun Si

School of Mechanical Electronic & Information Engineering, China University of Mining & Technology, Beijing 100083, China; dengjiaqingrae@163.com (J.D.); wangc@cumtb.edu.cn (C.W.); wushiyan_123@163.com (S.W.); oceanqueen1996@163.com (M.S.)

* Correspondence: chengh@cumtb.edu.cn

Received: 16 January 2020; Accepted: 5 February 2020; Published: 10 February 2020

Abstract: This paper presents an evaluation and comprehensive comparison for the topologies which are applied to the front stage of transformer-less cascaded multilevel converter (TCMC). The topologies investigated are targeted at the bidirectional cascaded H-bridge rectifier and three unidirectional rectifiers, including the diode H-bridge cascaded boost rectifier, cascaded bridgeless rectifier and cascaded VIENNA rectifier. First, the operation principles of the unidirectional rectifiers are discussed. Then the performances of these topologies such as power losses, efficiency, device current stress, cost, and total harmonic distortions are analyzed and evaluated respectively. Finally, advantages and disadvantages for each topology are discussed and highlighted. The evaluation and comparison methods presented in this paper and their results are feasible and effective for selecting the appropriate topology in practical applications under different operating conditions.

Keywords: unidirectional rectifier; bidirectional rectifier; comparison; power losses; efficiency; cost; current stress; THD analysis

1. Introduction

In recent years, with the rapid development of power semiconductor devices and power electronic technologies, the transformer-less cascaded multilevel converter (TCMC) has attracted extensive attention in the medium and high voltage application [1–7]. As shown in Figure 1, by employing the cascade H-bridge (CHB) converter as the front (last) stage, and the high-frequency isolated bidirectional DC-DC converter as the DC/DC stage, the TCMC can not only remove the bulky and expensive line-frequency transformer, but can also be connected directly to the medium/high voltage power grid and suited for the bidirectional power flow applications, such as coal mine hoists and locomotive traction, with some features as small size and light weight.

However, the TCMC mentioned above utilizes too many fully-controlled power switches (such as IGBTs or MOSFETs), making its main circuit and control system more complicated with higher cost and lower reliability. Considering that in many practical applications, bidirectional power flow is not always necessitated, such as in the Alternating Current (AC) speed regulation systems with pumps or fans load, etc., some researchers believe that in these applications, it might be a better choice to take the unidirectional rectifier like diode H-bridge cascaded boost rectifier, cascaded bridgeless rectifier and cascaded VIENNA rectifier as the front stage of TCMC [8–12]. The authors of [9] investigated the possibility of using the cascaded bridgeless rectifier to construct the front stage of TCMC. The authors of [10] discussed a method of using the diode H-bridge with the cascaded boost rectifier to construct the front stage of TCMC. The authors of [11] studied the cascaded single-phase VIENNA circuit and

the corresponding voltage balancing control strategy. The authors of [12] presented a hybrid cascading typology, in which the N bridgeless rectifiers and the M fully-controlled H-bridge rectifier are connected in cascading, causing the constructed front stage of TCMC to operate not only in unity power factor, but also in leading or lagging power factors. However, all the previous references are mainly directed at the power factor regulation and voltage balancing control, with no discussion about the comparison of comprehensive performance between these different unidirectional converter typologies, and between these different unidirectional rectifier typologies and H-bridge bidirectional rectifier-based TCMC, while the comprehensive performance comparison is very important for choosing the suitable typology to construct the TCMC in different industrial applications.

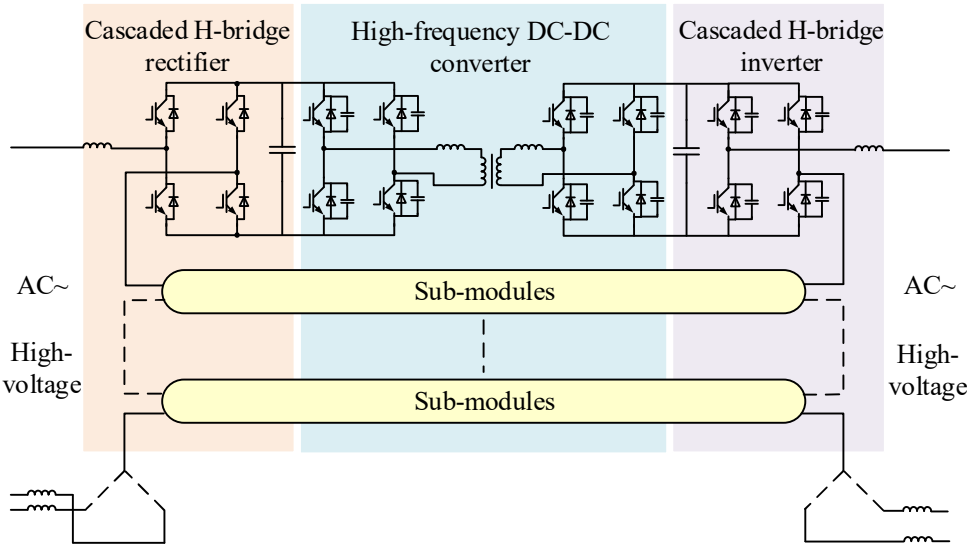

Figure 1. The main topology of the transformer-less cascaded H-bridge multilevel converter.

In this study, the topologies are focused on the bidirectional cascaded H-bridge rectifier, and three different kinds of topologies used in unidirectional power flow, including the diode H-bridge cascaded boost rectifier, the cascaded bridgeless rectifier, and the cascaded VIENNA rectifier. These topologies are compared on the basis of the theory of operation, power losses, efficiencies, device current stress, cost, and input current THD analysis. Moreover, it needs to be emphasized that in these topologies, identical hardware and parameters are utilized to ensure the objectivity and fairness of the comparison in this paper.

The remainder of the paper is organized as follows: Section 2 presents the configuration and the operation principle of these topologies. Section 3 discusses an investigation into the loss distribution of semiconductors and the efficiency comparison. Cost comparison is proposed in Section 4. Then the device stress and THD analysis are evaluated in Sections 5 and 6. Finally, conclusions are summarized in Section 7.

2. Description to Unidirectional Rectifier Topologies and Operation Principles

Since the cascaded H-bridge rectifier has already been a focus that attracts many scholars' attention and adopted in many practical applications [13–16], it will not be discussed in this section. Instead, the single-phase cascaded rectifiers with two modules in cascading will be taken as an example, and the structures and operation principles of the three types of unidirectional rectifiers will be analyzed.

2.1. Diode H-Bridge Cascaded Boost Rectifier

The diode H-bridge cascade boost rectifier is a novel cascaded multi-level rectifier which employs fewer fully-controlled switches and can achieve a unity power factor. Its structure is the combination

of a high voltage rated diode bridge D_1-D_4, and the cascaded boost DC/DC modules, as shown in Figure 2 [10,17].

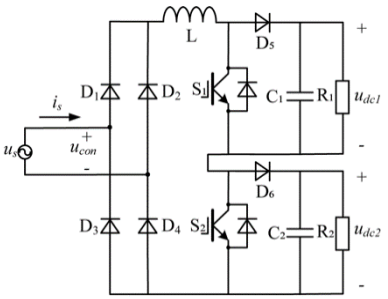

Figure 2. Single-phase diode H-bridge two-stage cascaded boost rectifier for transformer-less cascaded multilevel converter (TCMC).

S=1 is defined as the status when the fully-controlled power switch is turn-on, while S=0 is turn-off, and for two switches (S_1, S_2), there are four modes during the operation of the circuit, namely (1,1), (0,1), (1,0), (0,0). Because the positive and negative half cycles of the power supply voltage are symmetrical, only the positive half cycle is analyzed, and the current path of the four operation modes in the positive half period of AC voltage are shown in Figure 3.

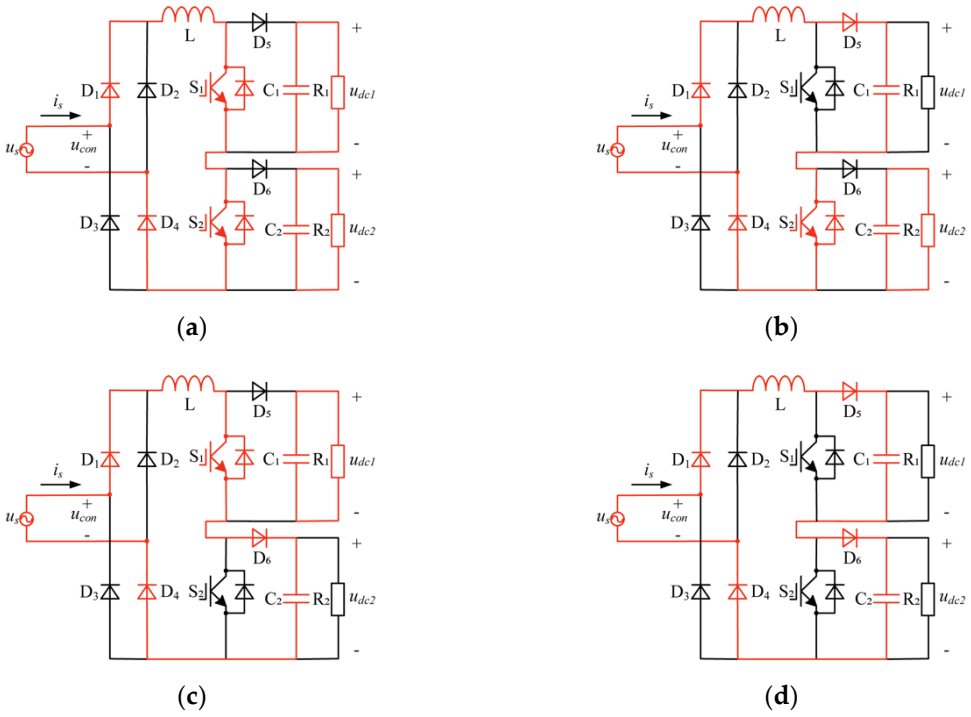

Figure 3. Current paths of the four operation modes for diode H-bridge two-stage cascaded boost rectifier; (**a**) Mode I; (**b**) Mode II; (**c**) Mode III; (**d**) Mode IV.

2.2. Cascaded Bridgeless Rectifier

As the bridgeless topology avoids the needs for the rectifier input diode bridge, and maintains the classic boost topology, it has been studied by many scholars and widely used in power factor correction (PFC) [18–22]. Furthermore, the bridgeless rectifier can be cascaded as the front stage of TCMC, as shown in Figure 4. Each module is composed of two fast recovery diodes D_1 and D_2, two active switches S_1 and S_2 with inherently body diodes D_{S1} and D_{S2}, and a capacitor C. With fewer active switches than H-bridge rectifier, and when compared with the diode H-bridge boost rectifier,

bridgeless rectifier can not only reduce the total number of switching devices by two, but also lessens the number of switching devices in the current path during normal operation in each module. Since the fast recovery diodes D_1 and D_2 are unidirectional conductive, the AC side combined voltage of the bridgeless rectifier is determined by the states of switches, and the polarity of the input current.

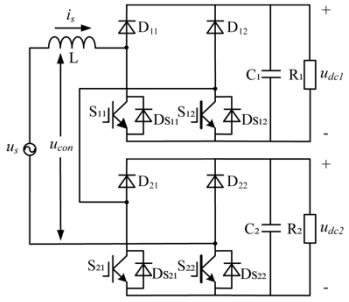

Figure 4. Single-phase two-stage cascaded bridgeless rectifier for TCMC.

The effective operation mode of the two-stage cascaded bridgeless rectifier can be divided into four modes according to the states of the four switches (S_{11}, S_{12}, S_{21}, S_{22}), namely (1, 1, 1, 1), (0, 0, 1, 1), (1, 1, 0, 0) and (0, 0, 0, 0). The four operation modes in the positive half period of AC voltage can be obtained in Figure 5.

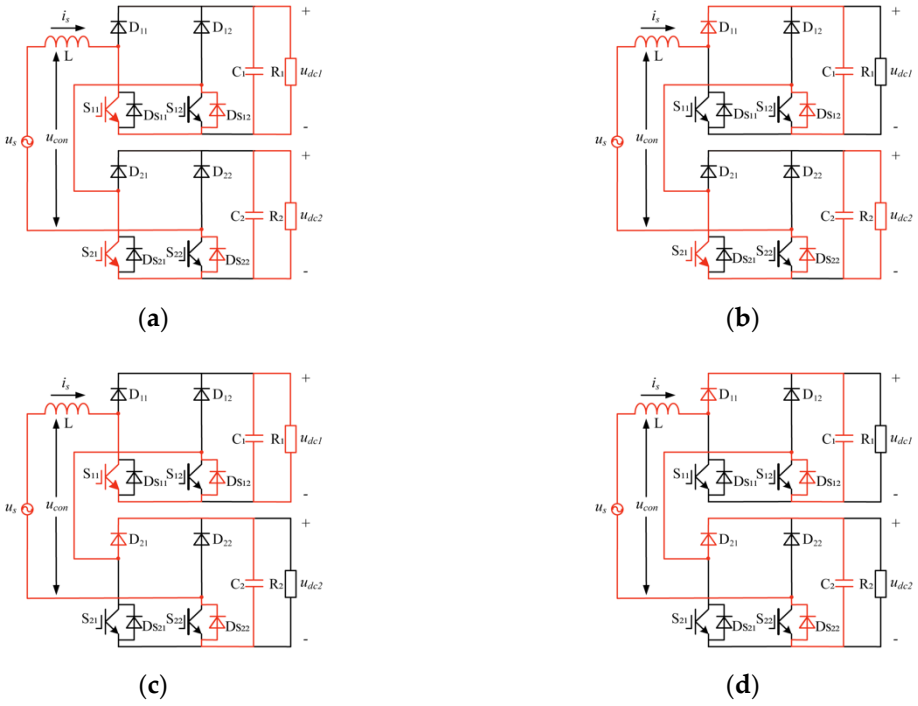

Figure 5. Current paths of the four operation modes for two-stage cascaded bridgeless rectifier; (**a**) Mode I; (**b**) Mode II; (**c**) Mode III; (**d**) Mode IV.

2.3. Cascaded VIENNA Rectifier

The cascaded VIENNA rectifier circuit is shown in Figure 6. Due to the structural characteristics of the VIENNA rectifier, one of the most important advantage for this topology is that each semiconductor device only suffers half of the total DC bus voltage [8]. As for the structure of a single module VIENNA topology, it is comprised of one input inductor L, two output capacitors C_1 and C_2, one active switch S, two regular diodes D_1 and D_3, and four fast recovery diode D_2, D_4, D_5 and D_6.

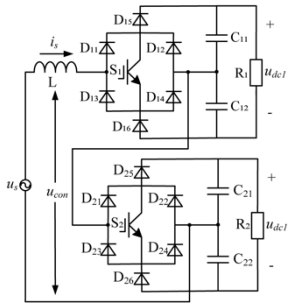

Figure 6. Single-phase two-stage cascaded VIENNA rectifier for TCMC.

Depending on the switching states of the (S_1, S_2), there exist four operation modes under positive half period for the two-stage cascaded VIENNA rectifier, as shown in Figure 7.

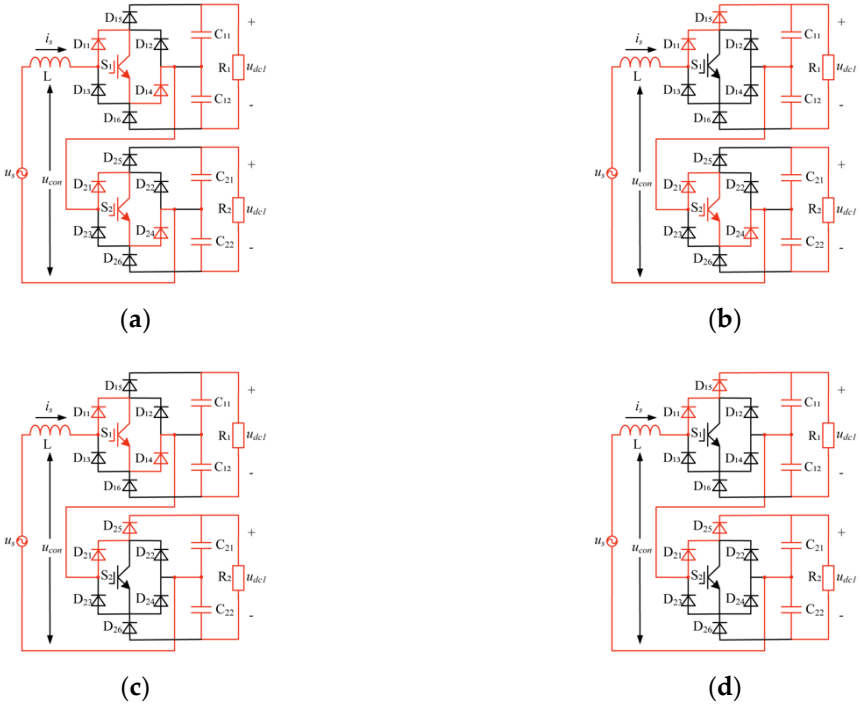

Figure 7. Current paths of the four operation modes for cascaded VIENNA rectifier; (**a**) Mode I; (**b**) Mode II; (**c**) Mode III; (**d**) Mode IV.

3. Power Losses and Efficiency-Based Evaluation

Since the power losses of the power semiconductor, including the conduction and switching losses are the major contributors to the rectifier losses, the total losses only take the semiconductor power losses into consideration in the following discussion. Analysis in this section will be implemented by PLECS software on the power loss distribution of the power semiconductors and the efficiency comparison in the four types of topologies as shown in Section 2, since PLECS software has been widely used in simulation on power electronics losses, on the basis of the component datasheet [23–25].

3.1. Calculation of Switching and Conduction Losses

(1) Calculation of IGBT losses

Switching losses are caused by the transition of the power devices between the blocking state and the conducting state, including turn-on losses and turn-off losses.

Accordingly, the switching losses P_{sw} can be expressed in (1) as:

$$P_{sw} = (E_{on} + E_{off}) \times f_{sw} \tag{1}$$

where E_{on} and E_{off} are the energy losses during the turn-on and turn-off of the switches and be read from a 3D look-up table, f_{sw} represents the switching frequency.

The conduction losses, caused by the on resistance of IGBTs, occur when the device is in full conduction mode. Those losses are computed by averaging the conduction losses in each switching cycle as shown in (2) as:

$$P_{con} = \frac{1}{T}\int_0^T [v_{ce}(t) \times i_{ce}(t) \times D(t)]dt \tag{2}$$

where v_{ce} is the forward voltage drop of the device, i_{ce} stands for the current flowing through the device during the conduction period, and they are calculated based on second order approximation from the 2D look-up table. D is the duty cycle, T is the switching period

So that the losses of a IGBT can therefore be described as:

$$P_{IGBT} = P_{sw} + P_{con} \tag{3}$$

(2) Calculation of diode losses

Diode losses involve conduction losses P_{conD} and reverse recovery losses P_{recD}. Because the turn-on time is very short and the diodes' reverse blockage current is very small, the turn-on losses and blockage losses can be neglected.

The reverse recovery losses of diode can be expressed as:

$$P_{recD} = E_{rr} \times f_{sw} \tag{4}$$

where E_{rr} indicates the turn-off losses of diode.

And the conduction loss calculation of the diode is similar to that of the switch. So the losses of a diode can be denoted as (5):

$$P_D = P_{\mathrm{rec}D} + P_{conD} \tag{5}$$

Thus, the total losses are calculated as follows:

$$P_{loss} = (P_Q + P_D) = (P_{sw} + P_{con} + P_{recD} + P_{conD}) \tag{6}$$

3.2. Investigation of Power Losses and Efficiency

In order to make a fair comparison, the same hardware and parameters have been used, as shown in Table 1.

Table 1. Rectifier Parameters.

Parameters	Type/Values
Input voltage (RMS)	380 V
Source voltage frequency	50 Hz
Switching frequency	10 KHz
DC-link voltage	1200 V
Load side capacitor	2200 mF
Input inductor	2 mH
Regular Diode (diode H bridge rectifier)	CS4112499C
Regular Diode (VIENNA rectifier)	60EPS12
Fast Diode	RHRG75120
IGBT	IGW60T120

Figure 8 shows the loss distribution of the power semiconductors in the four topologies investigated under the condition of *Po* = 6000 W.

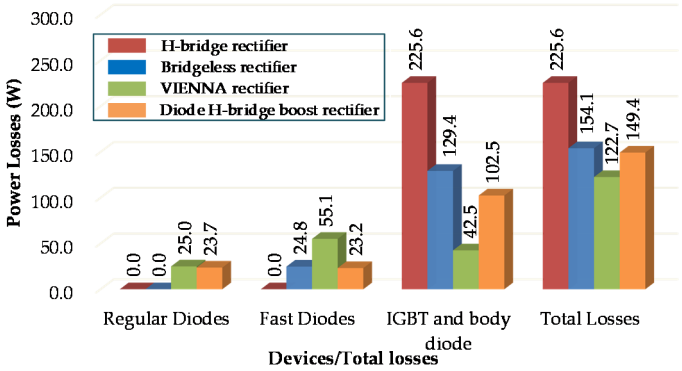

Figure 8. Loss distribution of the semiconductors.

From the graph above, it can be seen that the input diode bridge accounts for a part of the total losses among the cascaded VIENNA and diode H-bridge cascaded boost rectifiers, since the forward voltage drop of the diode bridge causes high conduction losses. Since the cascaded VIENNA rectifier has the lowest losses, due to the topological characteristics of the VIENNA rectifier, those semiconductor devices share only half of the DC bus voltage. The cascaded bridgeless rectifier and the cascaded H-bridge rectifier do not sustain the losses of diode bridge, while they have more fully-controlled switches, and the cascaded H-bridge rectifier has the largest losses. In light of the description of the previous section, the cascaded bridgeless rectifiers reduce half of the fully-controlled switches compared to cascaded H-bridges rectifiers, and the total losses are 31.7% lower than that of the cascaded H-bridge rectifier, and it also has proved that the use of fewer fully-controlled switches can do reduce the losses.

3.3. Efficiency Investigation under Different Power Loading

The efficiency measurement is shown in Figure 9, which illustrates the efficiency of the four topologies at different load.

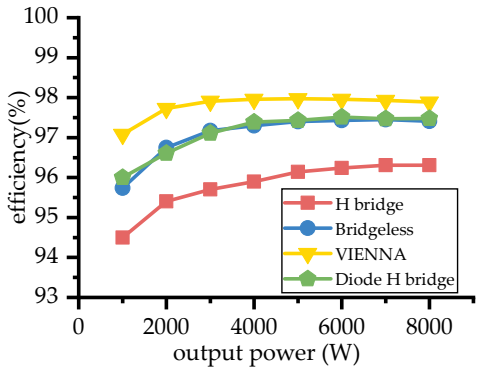

Figure 9. Efficiency versus output power for different rectifier.

It is obvious that the cascaded VIENNA rectifier always functions more efficiently than the other two unidirectional rectifiers and the bidirectional cascaded H-bridge rectifier, and can also achieve at a peak efficiency of 97.97%, whereas the efficiencies for the cascaded bridgeless rectifier and diode H-bridge cascaded rectifier are secondary to it. The cascaded H-bridge rectifier performs at the lowest efficiency.

4. Cost Performance Analysis

The differences in the main electrical power components used in N-stage cascaded single-phase topologies are illustrated in Table 2.

Generally speaking, the cost of these rectifiers depends mainly on the devices such as IGBT, diode, input inductor, and DC-link capacitor, etc. As can be seen from Table 3, the cost for the cascaded bridgeless rectifier is relatively lower, and the coat for the diode H-bridge cascaded boost rectifier is moderate, whereas the cost of the cascaded H-bridge rectifier and the cascaded VIENNA rectifier are relatively higher. Moreover, it should be noted that due to the fairness of the comparison in this paper, identical hardware is guaranteed to be utilized in these topologies. However, the semiconductor devices of the VIENNA rectifier only share half of the DC bus voltage, and accordingly the price for semiconductor devices with low withstand voltage may be decreased. Thus, the cost of VIENNA rectifier will be reduced in practical applications.

Table 2. Main electrical power component count for rectifier topologies.

Device	Cascaded H-Bridge Rectifier	Diode H-Bridge Cascaded Boost Rectifier	Cascaded Bridgeless Rectifier	Cascaded VIENNA Rectifier
Regular Diode	0	4	0	2N
IGBT	4N	N	2N	N
Fast Recovery	0	N	2N	4N
Diode Capacitor	N	N	N	2N
Inductor	1	1	1	1

N represents the number of cascades modules.

Table 3. Cost comparison of the four topologies.

Topology	Cost
Cascaded H-bridge rectifier	High
Diode H-bridge cascaded boost rectifier	Medium
Cascaded bridgeless rectifier	Low
Cascaded VIENNA rectifier	High

5. Component Stresses

In order to select and design the devices in practical applications, comparison and analysis on the stresses of devices with different topologies are conducted in this section under the following assumptions [26]:

(1) All the topologies are worked at CCM mode.
(2) These circuits are supplied by an ideal AC power source with 50 Hz frequency and operate at unity power factor.
(3) The output DC voltage is stable with no voltage ripple

The inductor current is assumed as:

$$i_L(\theta) = I_m \sin(\theta) \tag{7}$$

Then, the inductor current ripple is assumed to be half of the peak inductor current:

$$\Delta I_{RP} = \frac{1}{2}\frac{I_m}{2} \tag{8}$$

Therefore, the RMS current of inductor is:

$$I_{LRMS} = \sqrt{\frac{1}{\pi}\int_0^{\pi} |I_m|\sin(\theta)\|^2 + (\frac{1}{2\sqrt{3}}\Delta I_{RP})^2} = \sqrt{\frac{97}{48}}\frac{P_{in}}{U_m} \tag{9}$$

The duty cycle of the IGBT is given by:

$$\delta_{IGBT}(\theta) = 1 - \frac{U_s(\theta)}{U_{dc}} = 1 - \frac{U_m \sin(\theta)}{U_{dc}} \tag{10}$$

where U_s, U_m are the input voltage and the corresponding peak voltage, the Udc is the DC bus voltage.

The instantaneous current of IGBT is:

$$i_{IGBT}(\theta) = I_m \sin(\theta)(1 - \frac{U_m \sin(\theta)}{U_{dc}}) \tag{11}$$

So the RMS current of IGBT can be expressed as:

$$I_{IGBTRMS} = \sqrt{\frac{1}{\pi}\int_0^{\pi} \left[I_m |\sin(\theta)| (1 - \frac{U_m \sin(\theta)}{U_{dc}}) \right]^2 d\theta} \tag{12}$$

Then, the fast diode duty cycle is given by:

$$\delta_D(\theta) = \frac{U_S(\theta)}{U_{dc}} = \frac{U_m \sin(\theta)}{U_{dc}} \tag{13}$$

So, the instantaneous current and AVG current of diode can be expressed as:

$$I_D(\theta) = I_m \sin(\theta) \frac{U_S(\theta)}{U_{dc}} = I_m \sin(\theta) \frac{U_m \sin(\theta)}{U_{dc}} \tag{14}$$

$$I_{DAVG} = \frac{1}{\pi}\int_0^{\pi} I_m \sin(\theta) \frac{U_m \sin(\theta)}{U_{dc}} d\theta \tag{15}$$

The output capacitor current is calculated by:

$$I_{CRMS} = \frac{I_0}{\sqrt{2}} = \frac{\sqrt{2}}{2} \frac{P_0}{U_{dc}} \tag{16}$$

where I_0 represents the output current.

The RMS and AVG of other devices can also be calculated by the above algorithm. As a result, the device stresses for the four circuit topologies are shown in Tables 4 and 5.

Table 4. The component current stress of H-bridge rectifier and bridgeless rectifier.

Topology	H-Bridge Rectifier	Bridgeless Rectifier
Inductor (RMS)	$\sqrt{\frac{97}{48}} \frac{P_{in}}{U_m}$	$\sqrt{\frac{97}{48}} \frac{P_{in}}{U_m}$
Bridge Diode (AVG)	Not applicable	Not applicable
Fast Diode (AVG)	Not applicable	$\frac{1}{2} \frac{P_{in}}{U_{dc}}$
IGBT (RMS)	$\frac{P_{in}}{\sqrt{3} U_m U_{dc}} \sqrt{\frac{6\pi(3{U_m}^2 + {U_{dc}}^2) - 64 U_m U_{dc}}{\pi}}$	$\frac{P_{in}}{\sqrt{6} U_m U_{dc}} \sqrt{\frac{3\pi(3{U_m}^2 + 4{U_{dc0}}^2) - 64 U_m U_{dc}}{\pi}}$
IGBT Intrinsic Diode (AVG)	$\frac{1}{2} \frac{P_{in}}{U_{dc}}$	$\frac{1}{2} \frac{P_{in}}{U_{dc}}$
Output Capacitor Ripple	$\frac{\sqrt{2}}{2} \frac{P_0}{U_{dc}}$	$\frac{\sqrt{2}}{2} \frac{P_0}{U_{dc}}$

Table 5. The component current stress of diode H-bridge rectifier and VIENNA rectifier.

Topology	Diode H-Bridge Rectifier	VIENNA Rectifier
Inductor (RMS)	$\sqrt{\frac{97}{48}}\frac{P_{in}}{U_m}$	$\sqrt{\frac{97}{48}}\frac{P_{in}}{U_m}$
Bridge Diode (AVG)	$\frac{2}{\pi}\frac{P_{in}}{U_m}$	$\frac{1}{\pi}\frac{P_{in}}{U_m}$
Fast Diode (AVG)	$\frac{P_{in}}{U_{dc}}$	$\frac{4P_{in}}{U_m}-\frac{\pi P_{in}}{U_{dc}}$ *1 or $\frac{P_{in}}{U_{dc}}$ *2
IGBT (RMS)	$\frac{P_{in}}{\sqrt{6}U_mU_{dc}}\sqrt{\frac{3\pi(3{U_m}^2+4{U_{dc}}^2)-64U_mU_{dc}}{\pi}}$	$\frac{P_{in}}{\sqrt{3}U_mU_{dc}}\sqrt{\frac{6\pi(3{U_m}^2+{U_{dc}}^2)-64U_mU_{dc}}{\pi}}$
IGBT Intrinsic Diode (AVG)	Not applicable	Not applicable
Output Capacitor Ripple	$\frac{\sqrt{2}}{2}\frac{P_0}{U_{dc}}$	$\frac{\sqrt{2}}{4}\frac{P_0}{U_{dc}}$

*1 represent the current stresses of D_2 and D_4 in VIENNA topology. *2 represent the current stresses of D_5 and D_6 in VIENNA topology.

6. THD Analysis of Input Current

In order to better analyze the difference of total harmonic distortions (THD) of the input current between the bidirectional rectifier and the unidirectional rectifier, some simulations have been performed with MATLAB /Simulink software, the results at *Po* = 6 kW are shown in Figure 10. From the harmonic analysis of the input current, it is evident that the THD of the unidirectional rectifiers are generally higher than that of the bidirectional rectifier. Then the scaled-down experiment prototypes are built under *Po* = 1650 W. The experiment results show that the input current and voltage waveforms of three different types of unidirectional rectifiers are much the same. Taking the comparison between the cascaded H-bridge rectifier and the cascaded bridgeless rectifier as an example, as shown in Figure 11, it can be seen that the unidirectional rectifiers have the zero-crossing distortion of the input current. The cause of the distortion for the input current is analyzed below.

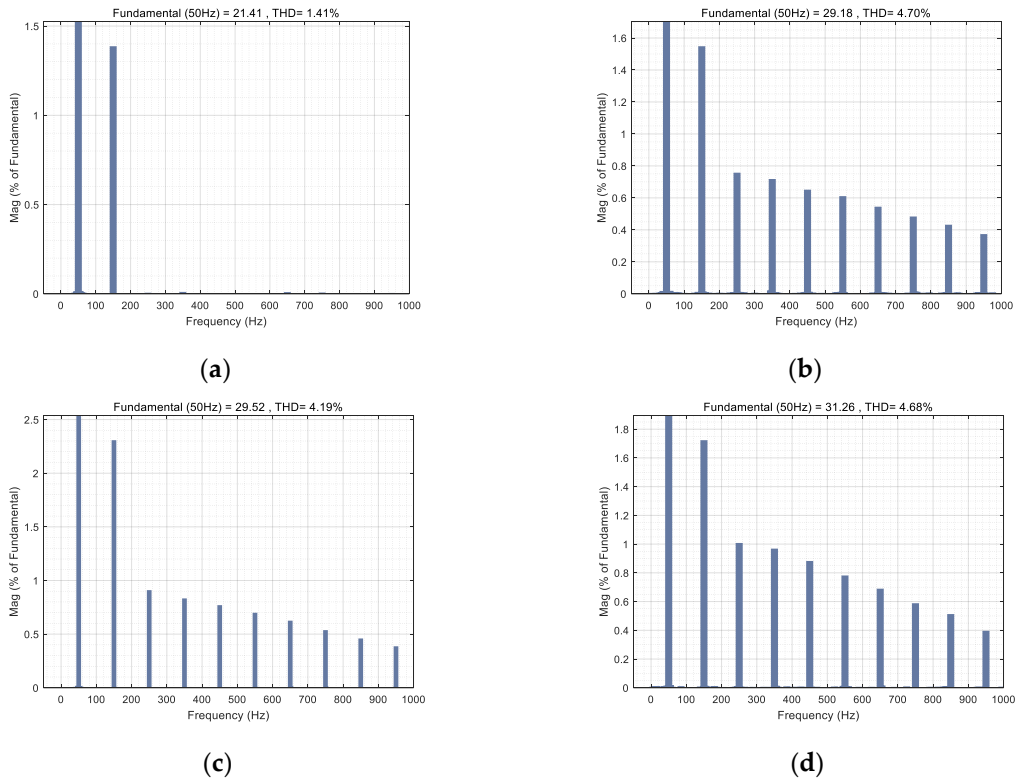

Figure 10. Input current Fourier decomposition; (**a**) H-bridge rectifier; (**b**) Bridgeless rectifier; (**c**) VIENNA rectifier; (**d**) Diode H-bridge boost rectifier.

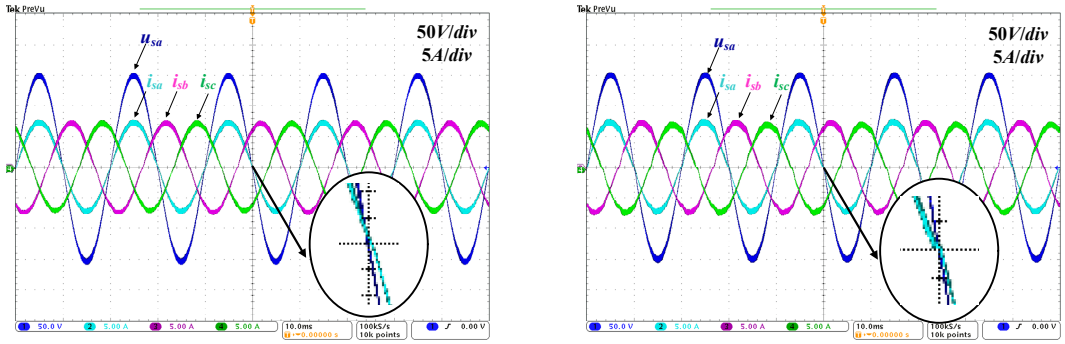

(**a**) (**b**)

Figure 11. Input current and input voltage waveforms (**a**) cascaded three-phase H-bridge rectifier; (**b**) cascaded three-phase bridgeless rectifier.

Figure 12 shows the AC side phasor diagram under unity power factor for the unidirectional rectifiers. The input voltage u_s is in phase with input voltage i_s, the voltage across the inductance u_L is orthogonal to i_s. According to the vector addition, the AC side reference voltage u^*_{con} lags the i_s by θ. Therefore, the u^*_{con} needs to be opposite to i_s during the period of θ as depicted in Figure 13. However, due to the unidirectional power flow, the polarity of input current i_s should be the identical to the AC voltage u_{con}, so u_{con} can only generate a zero AC voltage during the period of θ. After u^*_{con} changes from negative to positive, i_s can follow i^*_s after a period of γ [12,27]. The distortions of the input current will become more severe while the leading or lagging angle is increased, so the controllability angle for unidirectional rectifier is limited.

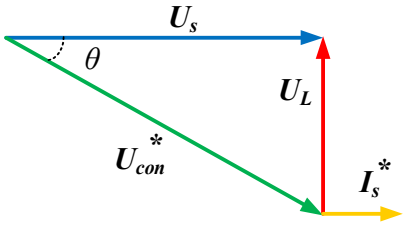

Figure 12. AC side phasor diagram of unidirectional rectifier.

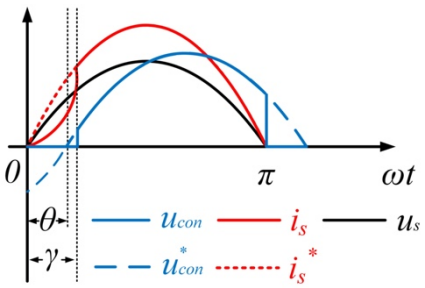

Figure 13. Waveform of voltage and current in AC side.

However, in order to improve the THD performance for the unidirectional topologies, the control methods have been modified to decrease the distortion of the input current, and to increase the controllability angle [28–30].

7. Conclusions

An evaluation and comprehensive comparison between unidirectional rectifiers and bidirectional rectifier are presented in this paper. The topologies discussed are centered on the cascaded bidirectional

H-bridge rectifier, and three different types of unidirectional rectifiers. The operation principle of the rectifiers, and their power losses, efficiencies, device stress, cost, and THD of the input current are analyzed and compared. The results show that each of the topologies possesses several advantages and disadvantages. Although the bidirectional rectifier exhibits the characteristic of low THD input current, and those types of topologies are appropriate for the bidirectional power flow application, its disadvantages cannot be neglected because of its fully-controlled power switches, resulting in higher power losses, greater cost and a more complicated control system. Meanwhile, unidirectional rectifiers also have many advantages, such as lower device stress, lower power losses, higher efficiency for the cascaded VIENNA rectifier, and lower cost for cascaded bridgeless rectifier, whereas their THD of the input current is relatively higher, so that their control systems must be carefully designed. The evaluation and comparison methods presented in this paper and their results are feasible and effective for selecting the appropriate topology in practical applications under different operating conditions.

Author Contributions: J.D., H.C. and C.W. conceptualized the main idea of this project; J.D. proposed the methods and designed the work; J.D. conducted the experiments and analyzed the data; S.W. and M.S. checked the results; J.D. wrote the whole paper; H.C. and C.W. reviewed and edited the paper. All authors have read and agreed to the published version of the manuscript.

Funding: This research was funded by the National Natural Science Foundation of China under Grant No. 51577187 and the Fundamental Research Funds for the Central Universities grant number 2010JY03.

Acknowledgments: This work was supported by the National Natural Science Foundation of China under Grant No. 51577187, and the Fundamental Research Funds for the Central Universities (2010JY03).

Conflicts of Interest: The authors declare no conflict of interest.

References

1. Akagi, H.; Inoue, S. Medium-Voltage Power Conversion Systems in the Next Generation. In Proceedings of the IEEE International Power Electronics and Motion Control Conference, Shanghai, China, 14–16 August 2006; pp. 1–8.
2. Iman Eini, H.; Farhangi, S.; Schanen, J.L. A modular AC/DC rectifier based on cascaded H-bridge rectifier. In Proceedings of the International Power Electronics and Motion Control Conference, Poznan, Poland, 1–3 September 2008; pp. 173–180.
3. Shi, J.; Gou, W.; Yuan, H.; Zhao, T.; Huang, A.Q. Research on voltage and power balance control for cascaded modular solid-state transformer. *IEEE Trans. Power Electron.* **2011**, *26*, 1154–1166. [CrossRef]
4. Dang, H.Q.S.; Watson, A.; Clare, J.; Wheeler, P.; Kenzelmann, S.; de Novaes, Y.R.; Rufer, A. Advanced integration of multilevel converters into power system. In Proceedings of the Annual Conference of IEEE Industrial Electronics, Orlando, FL, USA, 10–13 November 2008; pp. 3188–3194.
5. Huang, A.Q.; Crow, M.L.; Heydt, G.T.; Zheng, J.P.; Dale, S.J. The Future Renewable Electric Energy Delivery and Management (FREEDM) System: The Energy Internet. *Pron. IEEE.* **2011**, *99*, 133–148. [CrossRef]
6. Venkat, J.; Shukla, A.; Kulkarni, S.V. Operation of a three phase solid state-Transformer under unbalanced load conditions. In Proceedings of the IEEE International Conference on Power Electronics, Drives and Energy Systems, Mumbai, India, 16–19 December 2014; pp. 1–6.
7. Guo, P. Research on cascaded H-bridge rectifier stage and balance control for DC-link capacitor voltages. Ph.D. Thesis, China University of Mining and Technology, Beijing, China, 1 April 2012.
8. Zou, J.; Wang, C.; Cheng, H.; Liu, J. Triple Line-Voltage Cascaded VIENNA Converter Applied as the Medium-Voltage AC Drive. *Energies* **2018**, *11*, 1079. [CrossRef]
9. Cong, W.; Jian, J.; Chang, W.; Hong, C. Research on New Multi-level Cascaded Bridgeless Rectifier. *J. Power Supply* **2015**, *13*, 10–16.
10. Wang, C.; Wang, C.; Jiang, X.; Cheng, H. A Novel Cascaded Diode H-Bridge Multi-Level Rectifier. *Power Syst. Technol.* **2015**, *39*, 829–836.
11. Chen, H.; Wang, C.; Hu, H.; Liu, J.; Zhao, Z.; Zhang, Y.; Lu, Q.; Zou, J. DC Voltage Balance Control Strategy for Unidirectional Cascaded Multilevel Power Electronic Converter. China Patent Application No. CN109039129A, 18 December 2018.

12. Wang, C.; Zhuang, Y.; Jiao, J.; Zhang, H.; Wang, C.; Cheng, H. Topologies and Control Strategies of Cascaded Bridgeless Multilevel Rectifiers. *IEEE J. Emerg. Sel. Topics Power Electron.* **2017**, *5*, 432–444. [CrossRef]
13. Zanchetta, P.; Gerry, D.B.; Monopoli, V.G.; Clare, J.C.; Wheeler, P.W. Predictive Current Control for Multilevel Active Rectifiers With Reduced Switching Frequency. *IEEE Trans. Ind. Electron.* **2008**, *55*, 163–172. [CrossRef]
14. Moeini, A.; Zhao, H.; Wang, S. A Current-Reference-Based Selective Harmonic Current Mitigation PWM Technique to Improve the Performance of Cascaded H-Bridge Multilevel Active Rectifiers. *IEEE Trans. Ind. Electron.* **2018**, *65*, 727–737. [CrossRef]
15. Moosavi, M.; Farivar, G.; Iman-Eini, H.; Shekarabi, S.M. A voltage balancing strategy with extended operating region for cascaded H-bridge converters. *IEEE Trans. Power Electron.* **2014**, *29*, 5044–5053. [CrossRef]
16. Watson, A.J.; Wheeler, P.W.; Clare, J.C. A Complete Harmonic Elimination Approach to DC Link Voltage Balancing for a Cascaded Multilevel Rectifier. *IEEE Trans. Ind. Electron.* **2007**, *54*, 2946–2953. [CrossRef]
17. Chang, W. Novel High-Power Cascaded H-Bridge Multi-Level Rectifier. Ph.D. Thesis, China University of Mining and Technology, Beijing, China, 1 January 2016.
18. Huber, L.; Jang, Y.; Jovanovic, M.M. Performance Evaluation of Bridgeless PFC Boost Rectifiers. *IEEE Trans. Power Electron.* **2008**, *23*, 1381–1390. [CrossRef]
19. Jang, Y.; Jovanovic, M.M. A Bridgeless PFC Boost Rectifier with Optimized Magnetic Utilization. *IEEE Trans. Power Electron.* **2009**, *24*, 85–93. [CrossRef]
20. Petrea, C.; Lucanu, M. Bridgeless power factor correction converter working at high load variations. In Proceedings of the IEEE Computer Society, Iasi, Romania, 13–14 July 2007; pp. 621–624.
21. Lu, B.; Brown, R.; Soldano, M. Bridgeless PFC implementation using one cycle control technique. In Proceedings of the IEEE Applied Power Electronics Conference and Exposition, Austin, TX, USA, 6–10 March 2005; pp. 812–817.
22. Gopinath, M.; Prabakaran; Ramareddy, S. A brief analysis on bridgeless boost PFC converter. In Proceedings of the International Conference on Sustainable Energy and Intelligent Systems, Chennai, India, 20–22 July 2011; pp. 242–246.
23. Li, C.; Yang, T.; Kulsangcharoen, P.; Calzo, G.L.; Bozhko, S.; Gerada, C.; Wheeler, P. A Modified Neutral-Point Balancing Space Vector Modulation Technique for Three-Level Neutral Point Clamped Converters in High Speed Drives. *IEEE Trans. Ind. Electron.* **2018**, *66*, 910–921. [CrossRef]
24. Siddique, M.D.; Mekhilef, S.; Shah, N.M.; Sarwar, A.; Iqbal, A.; Tayyab, M.; Ansari, M. Low Switching Frequency Based Asymmetrical Multilevel Inverter Topology With Reduced Switch Count. *IEEE Access.* **2019**, *7*, 86374–86383. [CrossRef]
25. Choudhury, A.; Pillay, P.; Williamson, S.S. Discontinuous Hybrid-PWM based DC-link voltage balancing algorithm for a 3-Level neutral point clamped (NPC) traction inverter drive. *IEEE Trans. Ind. Appl.* **2016**, *52*, 3071–3082. [CrossRef]
26. Musavi, F.; Eberle, W.; Dunford, W.G. Efficiency evaluation of single-phase solutions for AC-DC PFC boost converters for plug-in-hybrid electric vehicle battery chargers. In Proceedings of the IEEE Vehicle Power and Propulsion Conference, Lille, France, 1–3 September 2010; pp. 1–6.
27. Liu, J.; Liu, Y.; Zhuang, Y.; Wang, C. Analysis to Input Current Zero Crossing Distortion of Bridgeless Rectifier Operating under Different Power Factors. *Energies* **2018**, *11*, 2447. [CrossRef]
28. Cheng, H.; Kong, J.; Wang, X.; Wang, P.; Chen, T.; Wang, C. Power factor adjustment and input current distortion mitigation for three-phase unidirectional rectifier. *IET Power Electron.* **2019**, *12*, 1816–1824. [CrossRef]
29. Cheng, H.; Chen, T.; Wang, C.; Wang, X.; Qin, X. Single-phase Bridgeless Rectifier with Capability of Power Quality Management. In Proceedings of the IEEE International Power Electronics and Application Conference and Exposition, Shenzhen, China, 4–7 November 2018; pp. 1–6.
30. Wang, C.; Liu, J.; Cheng, H.; Zhuang, Y.; Zhao, Z. A Modified One-Cycle Control for Vienna Rectifiers with Functionality of Input Power Factor Regulation and Input Current Distortion Mitigation. *Energies* **2019**, *12*, 3375. [CrossRef]